JOURNAL OF VIROLOGY, Dec. 2003, p. 13182–13193 Vol. 77, No. 24
0022-538X/03/$08.00+0 DOI: 10.1128/JVI.77.24.13182–13193.2003

Three-Dimensional Structures of the A, B, and C Capsids of Rhesus Monkey Rhadinovirus: Insights into Gammaherpesvirus Capsid Assembly, Maturation, and DNA Packaging

Xue-Kui Yu,[1] Christine M. O'Connor,[2] Ivo Atanasov,[1] Blossom Damania,[3,4] Dean H. Kedes,[2,5] and Z. Hong Zhou[1]*

Department of Pathology and Laboratory Medicine, University of Texas at Houston Medical School, Houston, Texas 77030[1]; Myles H. Thaler Center for AIDS and Human Retrovirus Research, Department of Microbiology,[2] and Department of Internal Medicine,[5] University of Virginia, Charlottesville, Virginia 22908; and Department of Microbiology and Immunology[3] and Lineberger Comprehensive Cancer Center,[4] University of North Carolina at Chapel Hill, Chapel Hill, North Carolina 27599

Received 18 April 2003/Accepted 14 July 2003

Rhesus monkey rhadinovirus (RRV) exhibits high levels of sequence homology to human gammaherpesviruses, such as Kaposi's sarcoma-associated herpesvirus, and grows to high titers in cell cultures, making it a good model system for studying gammaherpesvirus capsid structure and assembly. We have purified RRV A, B, and C capsids, thus for the first time allowing direct structure comparisons by electron cryomicroscopy and three-dimensional reconstruction. The results show that the shells of these capsids are identical and are each composed of 12 pentons, 150 hexons, and 320 triplexes. Structural differences were apparent inside the shells and through the penton channels. The A capsid is empty, and its penton channels are open. The B capsid contains a scaffolding core, and its penton channels are closed. The C capsid contains a DNA genome, which is closely packaged into regularly spaced density shells (25 Å apart), and its penton channels are open. The different statuses of the penton channels suggest a functional role of the channels during capsid maturation, and the overall structural similarities of RRV capsids to alphaherpesvirus capsids suggest a common assembly and maturation pathway. The RRV A capsid reconstruction at a 15-Å resolution, the best achieved for gammaherpesvirus particles, reveals overall structural similarities to alpha- and betaherpesvirus capsids. However, the outer regions of the capsid, including densities attributed to the Ta triplex and the small capsomer-interacting protein (SCIP or ORF65), exhibit prominent differences from their structural counterparts in alphaherpesviruses. This structural disparity suggests that SCIP and the triplex, together with tegument and envelope proteins, confer structural and potentially functional specificities to alpha-, beta-, and gammaherpesviruses.

Gammaherpesviruses are a group of DNA tumor viruses that collectively form a subfamily of the family *Herpesviridae* (41). The only two known human pathogens of this subfamily are Kaposi's sarcoma-associated herpesvirus (KSHV) and Epstein-Barr virus (EBV). These viruses are associated with lymphomas and other malignancies (9, 26). A distinctive feature of these viruses, compared with alphaherpesviruses, is that they are very restricted in the types of cells that they infect and do not grow well in cultures.

Although they vary widely in the types of cells that they infect, rates of multiplication, genome sizes, specific proteins, and pathogenesis, the virions of alpha-, beta-, and gammaherpesviruses share a characteristic architecture in which the double-stranded DNA genome is surrounded by an icosahedral capsid, a thick tegument layer, and a lipid bilayer envelope (see references 38 and 47 for reviews). Structural studies on alphaherpesvirus (such as herpes simplex virus type 1 [HSV-1]) and betaherpesvirus (such as cytomegalovirus [CMV]) have demonstrated that the capsid, approximately 1,300 Å in diameter, is a T = 16 icosahedron with 12 pentons forming the vertices, 150 hexons forming the faces and edges, and 320 triplexes interconnecting the pentons and hexons. Central to pathogenesis and lytic HSV-1 infection is the well-coordinated assembly process leading to subviral particles (procapsids and A, B, and C capsids) and infectious virions. The A, B, and C capsids are stable enough to be readily isolated from the nuclei of HSV-1-infected cells or, alternatively, from the extracellular media after cell lysis.

Due to the lack of efficient cell culture systems, it remains difficult to obtain large quantities of purified capsids representative of different stages of viral assembly from KSHV and EBV; this problem has consequently hampered studies of the capsid assembly and structure of these viruses. Previously, KSHV A, B, and C capsids were isolated by chemical induction of latently infected BCBL-1 cells, a cell line derived from a primary effusion lymphoma (27). Three-dimensional (3D) reconstructions by electron cryomicroscopy (cryoEM) of KSHV capsids at a 24-Å resolution showed striking similarities to those of HSV-1 capsids, except for the small capsomer-interacting protein (SCIP or ORF65) (24, 51, 56). However, difficulties in obtaining adequate amounts of purified capsids for cryoEM analyses have prevented direct 3D structural comparisons of different capsid types. Reconstructions by cryoEM have been carried out only for either the "empty" A capsids or for a mixture of A, B, and C capsids, and the resolutions have

* Corresponding author. Mailing address: Department of Pathology and Laboratory Medicine, University of Texas at Houston Medical School, Houston, TX 77030. Phone: (713) 500-5358. Fax: (713) 500-0730. E-mail: z.h.zhou@uth.tmc.edu.

been limited to 24 Å (51, 56). Consequently, knowledge about the assembly and maturation of KSHV and of the gammaherpesviruses in general remains limited and often can be inferred only from an understanding of the alphaherpesviruses.

KSHV and rhesus monkey rhadinovirus (RRV) share a high degree of similarity with respect to transcription programs, genomic organization, and sequences (1, 15, 16, 45). Specifically, the sequence similarities between their capsid proteins range between 49 and 84% (sequence identities in the range of 40 to 70%) (35a). Moreover, analyses of all sequences currently deposited at The Protein Data Bank indicate that proteins with over 30% amino acid sequence identities often possess nearly identical 3D structures, sometimes up to the level of atomic resolution (3). Thus, it is reasonable to expect that the 3D structures of the RRV and KSHV capsids are markedly similar, particularly at the molecular resolution level (~10 to 20 Å). In contrast to KSHV, however, RRV grows to high titers in rhesus fibroblasts after de novo infection in cultures, facilitating the isolation of highly purified preparations of each of the capsid species (35a). As a result, RRV provides an attractive system for systematic studies of gammaherpesvirus structure and assembly.

In this study, we subjected purified RRV A, B, and C capsids to cryoEM structural analyses. Direct 3D structural comparisons of the A, B, and C capsids revealed differences in the penton channels and interiors of the capsids, suggested functional roles of the penton channels during capsid maturation, and indicated that gammaherpesvirus capsids mature in a pathway similar to that of capsids of HSV-1, the prototype of the alphaherpesvirus subfamily. In addition, we have determined the RRV A capsid structure to a 15-Å resolution, the highest to date for a gammaherpesvirus particle, and have found major structural variations in triplexes situated at quasi-equivalent positions. Moreover, the Ta triplex and structures located at the outer regions of the capsid, where SCIP binds, exhibit features significantly different from those observed in alpha- and betaherpesvirus capsids. This structural disparity suggests that SCIP and the triplex, together with tegument and envelope proteins, confer structural and potentially functional specificities to alpha-, beta-, and gammaherpesviruses.

MATERIALS AND METHODS

Purification of capsids. Cell cultures, RRV infection, capsid purification, and biochemical characterization are described in detail elsewhere (35a). Briefly, the viral capsid-containing supernatant was collected by low-speed centrifugation of the media from RRV-infected telomerase-immortalized rhesus monkey fibroblasts at 8 to 10 days postinfection, when severe cell lysis was observed. The capsids were pelleted, and Triton X-100 (Fisher Chemicals, Suwanee, Ga.) was added to a final concentration of 2% for overnight incubation at 4°C. The mixture was briefly bath sonicated at 4°C and sedimented (75,000 × *g* for 30 min in a Sorvall SW55Ti apparatus) through a 35% (wt/vol) sucrose cushion in 20 mM Tris-HCl (pH 8.0)–250 mM NaCl–1 mM EDTA (MTNE). The resulting pellet was resuspended, sonicated as described above, and loaded onto a 600-μl 20 to 50% sucrose– MTNE gradient. The gradient was centrifuged at 75,000 × *g* for 40 min in a Sorvall SW55Ti apparatus, and fractions (20 to 35 μl) were collected by bottom puncturing. Gradient fractions containing the three capsid species, as determined by electron microscopy and protein analyses (35a), were diluted in equal volumes of MTNE and centrifuged for 1 h at 4°C in a Sorvall ST-MICRO rotor at 42,300 × *g* to remove the sucrose. The resulting pellet was resuspended in 20 μl of MTNE and subjected to sodium dodecyl sulfate (SDS)-polyacrylamide gel electrophoresis (PAGE) analyses and cryoEM imaging.

CryoEM and 3D reconstruction. CryoEM imaging of RRV capsids was performed as described previously (56). Briefly, a 3-μl aliquot of purified RRV capsids was applied to a Quantifoil R 2/1 grid (Quantifoil Micro Tools Gmbh, Jena, Germany), quickly blotted with filter paper, and plunged into liquid nitrogen-cooled ethane so that the capsid particles were embedded in a thin layer of vitreous ice across the holes of the supporting film. Images were recorded at a magnification of ×30,000 and 100 kV in a JEOL 1200 electron cryomicroscope equipped with a liquid nitrogen-cooled cryospecimen holder (Gatan Inc., Pleasanton, Calif.) by using an electron dose of ~10 electrons/Å^2/micrograph. Focal pairs of cryoEM micrographs were recorded, with the first, close-to-focus micrograph aimed at ~1.0 μm under focus and the second, far-from-focus micrograph aimed at ~2 μm under focus.

Selected micrographs in the proper defocus range and without apparent specimen drift and charging were digitized on a Zeiss SCAI microdensitometer (Z/I Imaging, Huntsville, Ala.) by using a step size equivalent to 4.67 Å/pixel on the specimen. Data processing and visualization were carried out with SGI Octane workstations and an Origin 300 server (Silicon Graphics, Inc.) by using Fourier common-lines-based procedures implemented in the IMIRS package as previously described (21, 62). The defocus values of the micrographs were determined by using the incoherently averaged Fourier transforms of particle images (61). The orientation and center estimation and refinement were based on the focal-pair method (58). In this method, the particles from the far-from-focus micrographs were used to determine the initial orientation parameters of the corresponding particles from the close-to-focus micrographs, which were subsequently refined. The final 3D reconstructions were generated by merging only the close-to-focus particles (defocus values ranging from 0.8 to 2.1 μm) by using the Fourier-Bessel synthesis method (13) with correction of the contrast transfer function (57). The effective resolution was based on the criterion of the Fourier shell correlation coefficient being larger than 0.5 between two independent reconstructions from arbitrarily split data sets. 3D visualization was carried out by using Iris Explorer (NAG Inc., Downers Grove, Ill.) with custom-designed modules (17). All structures were displayed at a contour level of 1 standard deviation above the average density.

RESULTS

CryoEM of RRV A, B, and C capsids. The protein compositions of purified RRV A and C capsids are the same but are different from that of B capsids, as revealed by SDS-PAGE (Fig. 1) and characterized in detail by O'Connor et al. (35a). Like those of HSV-1, each of the capsid types has four abundant proteins: the major capsid protein (MCP or ORF25), the triplex monomer protein (TRI-1 or ORF62), the triplex dimer protein (TRI-2 or ORF26), and SCIP (or ORF65). B capsids additionally contain large amounts of the scaffolding protein (SCAF or ORF17.5). The relative molecular weights of these RRV capsid proteins are nearly identical to those of their homologs in KSHV (27) and, except for TRI-1, are similar to those in HSV-1 (29, 30, 39). RRV TRI-1 is significantly smaller than its HSV-1 counterpart, 50-kDa VP19C.

The cryoEM images of RRV A, B, and C capsids revealed typical features seen in other herpesvirus capsids characterized to date (Fig. 2). All three capsid types have a polyhedral shape with capsomers protruding from the outer rim of the polyhedron. The electron opacities revealed in the cryoEM images differ in the A, B, and C capsids, like those in other herpesvirus capsids. The A capsid images revealed the least electron opacity, suggesting that A capsids are empty shells (Fig. 2A). The B capsids contain a density core with a diameter of ~600 Å (Fig. 2B). The interior of the C capsids (Fig. 2C) is the most electron opaque of the three types of capsids, with internal densities completely obscuring the boundary of the internal capsid shell that, in contrast, is readily apparent in both the A and the B capsids. These electron-opaque internal densities inside the C capsids had the characteristic "fingerprint" appearance when the micrographs were recorded under close-to-focus conditions (Fig. 2C, insets), suggesting the presence of densely pack-

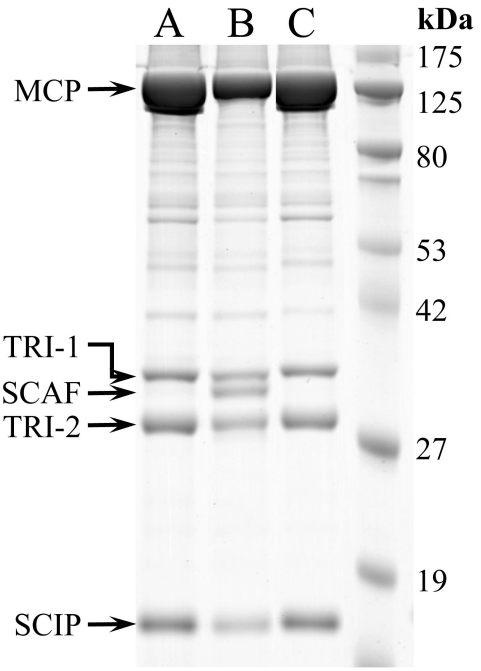

FIG. 1. Coomassie blue-stained gel of purified RRV A, B, and C capsids. RRV A, B, and C capsids were separated by velocity sedimentation (see Materials and Methods). Fractions containing the purest populations of A, B, and C capsids were subjected to SDS-PAGE and visualized by staining with Simply Blue Safe Stain (Invitrogen). Arrows indicate the bands of the five main capsid-associated proteins. The faint bands between MCP and TRI-1 are contaminating cellular proteins because they were also present in the density gradient fractions containing no capsids. The stoichiometry of TRI-1 and TRI-2, as estimated from the stain densities in the C capsid lane, was approximately 1:2.

aged double-stranded DNA (dsDNA), as also reported for HSV-1 C capsids (5).

3D structural comparisons of A, B, and C capsids. The 3D structures of RRV A, B, and C capsids were reconstructed to effective resolutions of 15, 27, and 21 Å by combining 3,824, 320, and 450 A, B, and C capsid particle images, respectively. For direct comparisons, we first scaled all three structures to the same resolution of 27 Å (Fig. 3A), the best resolution achieved for the B capsid reconstruction because of the limited number of B capsid images. The shaded surface representations of these 3D reconstructions of the three capsid types are almost indistinguishable, revealing a T=16 icosahedral lattice that is common to the capsids of all herpesviruses examined to date (Fig. 3A). Each capsid contains 12 pentons located at the icosahedral vertices, 150 hexons on the triangular faces and edges, and 320 triplexes interconnecting the pentons and hexons (Fig. 3A). The internal views, however, reveal substantial differences (Fig. 3B). The inside of the A capsids is essentially empty, with only a trace of small densities at the center; these may reflect the presence in the preparation of a few contaminating B capsids, which are sometimes difficult to distinguish from A capsids in cryoEM micrographs. The B capsid reconstruction contains a 600-Å-diameter core of largely disordered densities. This core of densities can be divided into approximately three distinct radial layers. The inner layer is a solid sphere with a diameter of about 320 Å. The middle layer is a 110-Å-thick shell of continuous density that is extensively associated with the inner core. The outer layer consists of less robust densities projecting from the middle shell. No connection of this outer layer with the capsid floor is apparent, even when the images are displayed at a substantially decreased density threshold. The densities inside the C capsid, in contrast, are organized into evenly spaced spherical shells (Fig. 3B and Fig. 4; also see below).

Comparisons of penton and hexon channels in A, B, and C capsids. Despite the overall similarities of the capsomers within the capsid shells, the reconstructions revealed a subtle, yet intriguing difference inside the penton channels of the A, B, and C capsids. Both the penton ("5" in Fig. 3A) and the hexon ("H" in Fig. 3A) (Fig. 5B) have a cylindrical shape with an axial channel connecting the interior of the capsid to the exterior. By analogy to other herpesvirus capsids, we propose that RRV pentons and hexons contain five and six copies of the MCP, respectively. In the A capsids, the diameters of the penton channels vary at different radial positions from the center of the capsids (Fig. 3C and D) (for example, the diameters are 22 Å at the innermost radial position, 28 Å at the middle position, and 36 Å at the outermost position) and differ markedly from those of the hexon channels, which measure 34, 24, and 36 Å at the innermost, middle, and outermost radial positions, respectively (Fig. 5B). Whereas all hexon channels are identical in the A, B, and C capsids, penton channels exhibit marked differences, being open in both A and C capsids but shut near the midpoint of the channels in B capsids (Fig. 3D, arrow). The narrowest regions of the open penton channels in the A and C capsids are the same, both being ~22 Å in diameter.

Organization of viral DNA inside C capsids. The most striking feature of the C capsid reconstruction at a 21-Å resolution is the presence of evenly spaced density shells that extend internally toward the center of the capsid (Fig. 4). Because the protein compositions of A and C capsids are the same (Fig. 1) and their only chemical difference is the presence of the viral dsDNA genome inside C capsids (35a), we attribute these internal densities to the viral dsDNA. At least six spherical shells of densities can be distinguished before the densities gradually become featureless with further progression toward the center (Fig. 4A). The distance between adjacent DNA density shells was estimated to be 25 Å from the peaks in the radial density distribution obtained by spherically averaging the mass densities of the C capsid reconstruction (Fig. 4B). This spacing between adjacent dsDNA shells is similar to those inside bacteriophages P22 and lambda (18) but slightly smaller than the 26-Å spacing in HSV-1 virions, determined from a 20-Å map (57), and larger than the 23-Å packaging spacing of human CMV DNA, estimated from cryoEM images of human CMV virions (4).

Because icosahedral symmetry was imposed in our 3D reconstruction, the detailed structural features of the DNA densities revealed in our 3D reconstruction are difficult to interpret. However, the structural features of the DNA densities in the regions near the capsid floor may have some level of symmetry, at least at a low resolution, as a result of interactions with the capsid shell proteins. Consistent with this notion, we found that the DNA densities closer to the capsid floor are more ordered than those near the capsid center (Fig. 4A). The

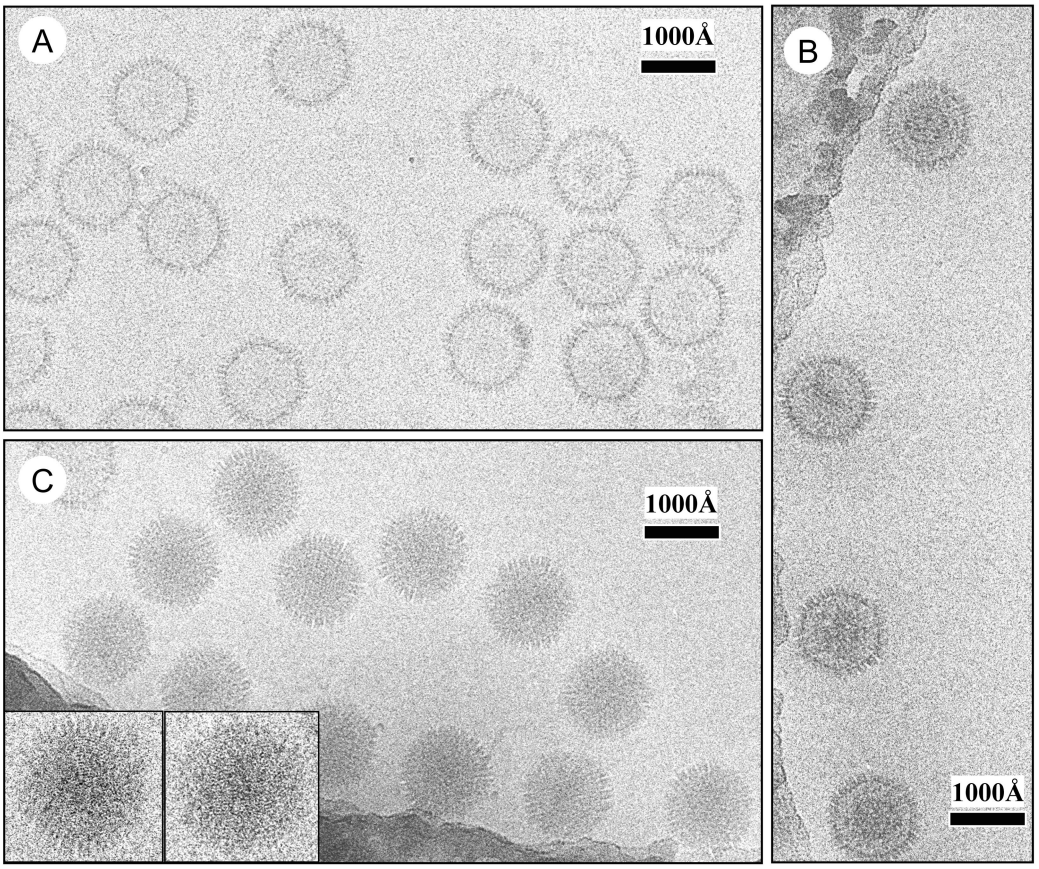

FIG. 2. CryoEM micrographs of RRV capsids. Purified RRV A capsids (A), B capsids (B), and C capsids (C) were embedded in vitreous ice and subsequently imaged in a JEOL 1200 electron cryomicroscope operated at 100 kV. The A capsid appears empty, the B capsid contains an inner core, and the C capsid has a striated, fingerprint appearance that results from the presence of the densely packaged dsDNA genome, which can be readily recognized in the close-to-focus particle images shown in the insets. All three capsid types have a polyhedral shape with characteristic capsomer protrusions, similar to those seen in HSV-1 and human CMV.

DNA layers are not perfectly spherical but rather are angular or polyhedral, adopting a shape that loosely parallels that of the surrounding capsid floor. Thus, it seems that the capsid floor may play an important structural role as a DNA packaging scaffold or constraint. This constraint maintains the energetically unfavorable organization of the linear dsDNA genome within the capsid. In this regard, it is relevant to point out that the outermost layer of dsDNA exhibits numerous interactions with the overlying floor domains of MCP molecules, including the strongest of these near the fivefold axes and the less prominent of these near the three- and twofold axes (Fig. 4A). It is conceivable that these interactions exert considerable constraints on the first shell of packaged DNA to adapt the same polyhedral shape as the inner floor of the capsid (Fig. 4A). The polyhedral contour continues within the second DNA shell and beyond and only gradually disappears within the sixth shell. This mirroring of the layers of DNA strands probably reflects the close packaging of the viral genome, which is constrained by the limited space of the rigid capsid (see Discussion).

Protein subunits on the capsid shell. Among our preparations, the A capsids were the most abundant capsid species and were thus reconstructed to the highest resolution among the three capsid forms. From 3,824 particles, the final effective resolution of the A capsid reconstruction reached 15 Å, the best resolution ever achieved for a gammaherpesvirus capsid (Fig. 5A). This 15-Å structure has allowed us to dissect individual structural components computationally for more detailed analyses (Fig. 5B) and comparisons with the capsid structures of other herpesviruses. Whereas subunits computationally extracted from a penton and an E hexon, together with its associated triplex, have similar elongated overall shapes, with upper, middle, lower, and floor domains, there were some minor differences between the penton and the hexon subunits (Fig. 5C). The most dramatic of these differences is that the angles between the floor domains and the long axes of the penton and hexon subunits are 110° and 90°, respectively. Consequently, the penton is slightly longer than the hexon (162 versus 156 Å) (Fig. 5C). These structural changes in the penton and the hexon in RRV MCP were also observed in HSV-1 (see Fig. 5D and F in reference 56), although notable differences between the MCP molecules of HSV-1 and RRV were also apparent (Fig. 6).

In addition to their slightly shorter length, the hexons appear to be more compactly arranged than the pentons (Fig. 5B), probably due to the requirement for packaging one additional

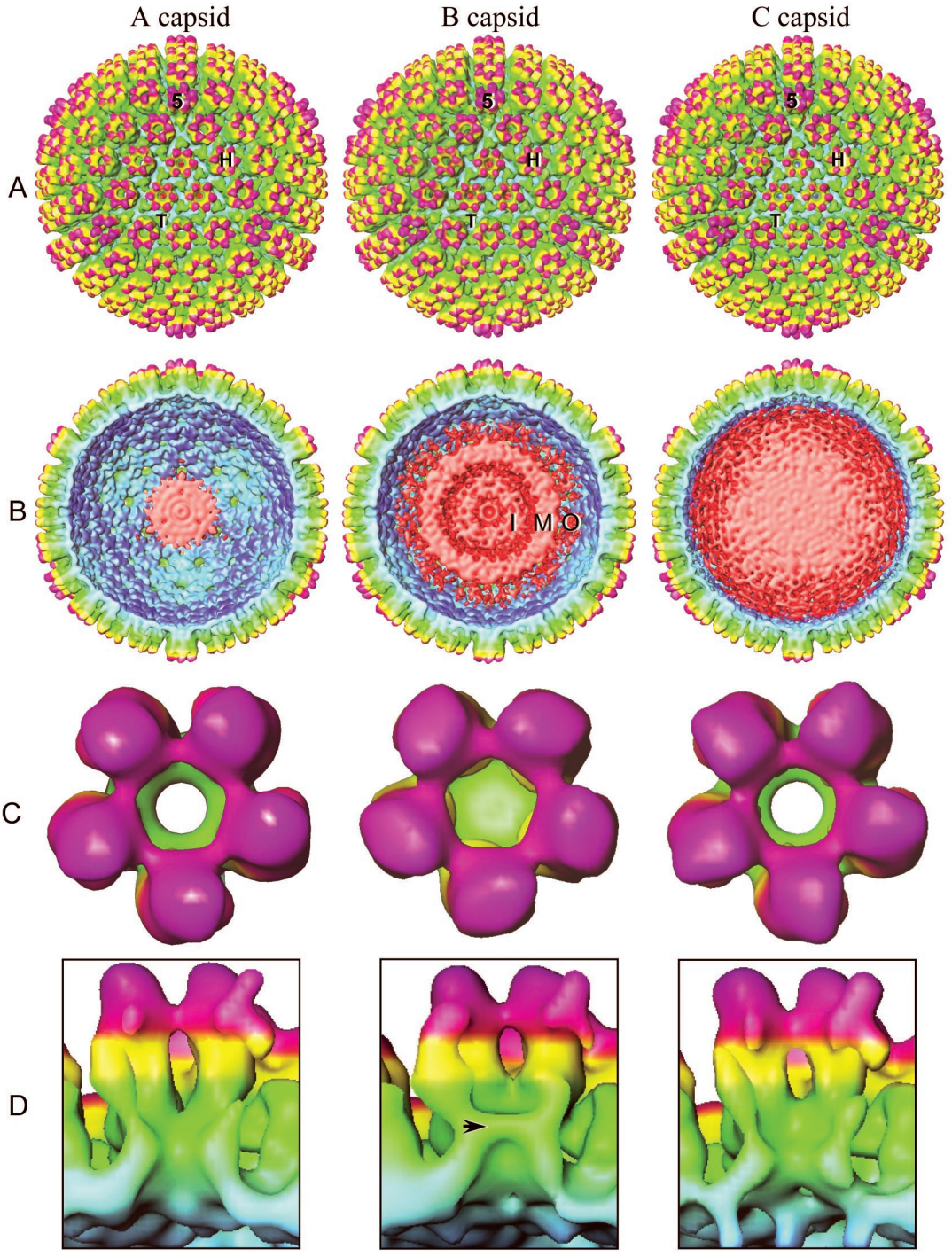

FIG. 3. Structural comparisons of RRV A, B, and C capsids at 27-Å resolution. The 3D maps are colored according to particle radius, such that the capsid floor is in aquamarine, the triplexes are in green, the middle domains of the pentons and hexons are in yellow, and the upper domains of the pentons and hexons are in purple. (A) Shaded surface representations of RRV capsids viewed along an icosahedral threefold axis. The A (left), B (middle), and C (right) capsids have almost identical surface features, each composed of 12 pentons (denoted by 5), 150 hexons (denoted by H), and 320 triplexes (denoted by T) arranged on a T=16 icosahedral lattice. (B) Cutaway views of RRV capsids viewed along a threefold axis, revealing the density differences inside the capsid shell. The A capsid is almost empty. The B capsid contains a 600-Å-diameter core of disordered densities arranged in three distinct radial regions: inner (I), middle (M), and outer (O). The C capsid is full of densities attributed to the densely packaged dsDNA genome. (C and D) Comparisons of penton channels. The close-up top views along the fivefold axis (C) of the computationally extracted pentons and the cutaway side views (D) reveal that the penton channels in the A and C capsids are open, while that in the B capsid is shut (arrow).

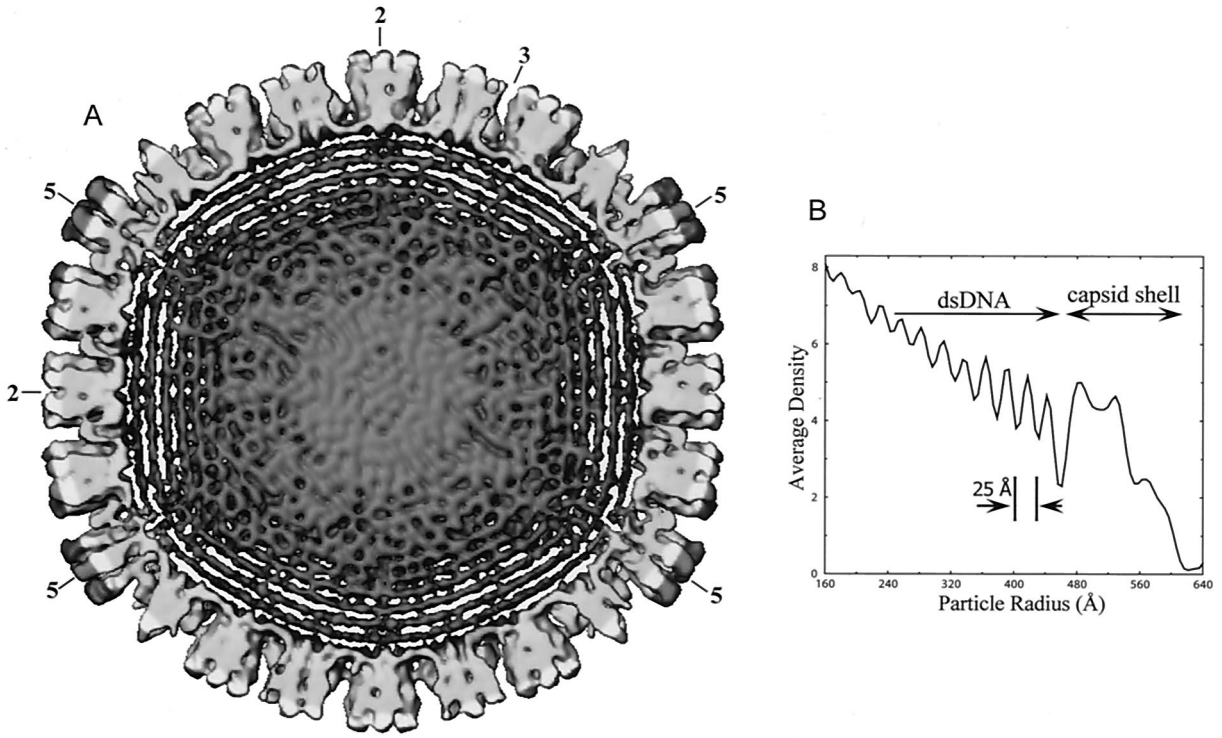

FIG. 4. Packaging of dsDNA inside the C capsid. (A) A 100-Å-thick central slice extracted from the 21-Å resolution of the C capsid reconstruction is shown along a twofold axis. The slice exhibits high-density features organized as multiple spherical shells inside the inner surface of the capsid floor. At least six concentric shells can be distinguished before the pattern becomes indistinct toward the center of the capsid. (B) Radial density distribution of the C capsid obtained by spherically averaging the C capsid reconstruction. It is evident that the distance between neighboring peaks is about 25 Å. "2", "3", and "5" represent icosahedral 2-, 3-, and 5-fold axes.

subunit within cylindrical spaces with similar diameters (140 and 136 Å for hexons and pentons, respectively). With the exception of the interconnections between the upper domains, the penton subunits are well separated from each other. Unlike HSV-1, whose hexon subunit (but not penton subunit) has a horn-shaped density due to the presence of VP26 on the upper domains of the hexons (52, 62, 64) (see Fig. 5D and F in reference 56), the corresponding regions of RRV pentons and hexons have similar shapes (cf. Fig. 5C and D and Fig. 5D and F in reference 56). Nevertheless, the superposition of the penton and hexon subunits reveals an extra density, albeit less prominent than the horn-shaped density in the HSV-1 hexon, on top of the upper domain of the RRV hexon subunit (Fig. 5C). This small extra density may represent a portion of SCIP or ORF65, the VP26 homolog in RRV.

Each triplex has a pyramidal shape with three legs pointing toward the capsid floor; each of the legs makes variable numbers of contacts with the capsid floor (Fig. 5B, right, and Fig. 5C). The three legs are positioned around a small hole on the capsid floor. One of these legs (L3 in Fig. 5B) extends to form the bulk of the upper domain of each triplex and remains continuous even when the map is displayed at a high density threshold (data not shown). The other two legs (L1 and L2 in Fig. 5B) resemble each other and intertwine under the upper domain of the triplex. Except for Tf, the upper domain of each triplex has two protrusions, one "head" and one "tail" (Fig. 5B, right), extending sideways to connect with the middle and the lower domains of adjacent capsomer subunits, respectively. Although the triplexes have similar overall structures, there are some minor differences among them because of their different (or quasi-equivalent) local environments. Triplex Tf is located at the threefold axis, thus having a perfect threefold symmetric shape. Ta differs from Tb, Tc, Td, and Te in that two of its three legs (L2 and L3) are completely disconnected from the capsid floor (Fig. 5A and C).

DISCUSSION

Implications for gammaherpesvirus capsid assembly and maturation. Among the three subfamilies of the *Herpesviridae*, the alphaherpesviruses are the best structurally characterized (reviewed in references 38 and 47); these include equine herpesvirus 1 (2) and the extensively studied HSV-1 (5, 31, 32, 42, 43, 48–50, 52, 53, 62–64). Although none of these studies documented the comparisons of all three types of capsids, as done in our current gammaherpesvirus study, correlations between the reported structures and assembly results have led to our current understanding of alphaherpesvirus assembly. In HSV-1, capsid assembly begins with the formation of a spherical procapsid through the association of the C terminus of the scaffolding protein with the N terminus of MCP (19, 54, 55), similar to the bacteriophage prohead (31, 35, 40, 50). The procapsid is unstable and exists only transiently before transforming into the stable angular or polyhedral shape of the B capsid (35, 40, 63). Cells infected with a mutant HSV-1 strain containing a temperature-sensitive lesion in the protease pro-

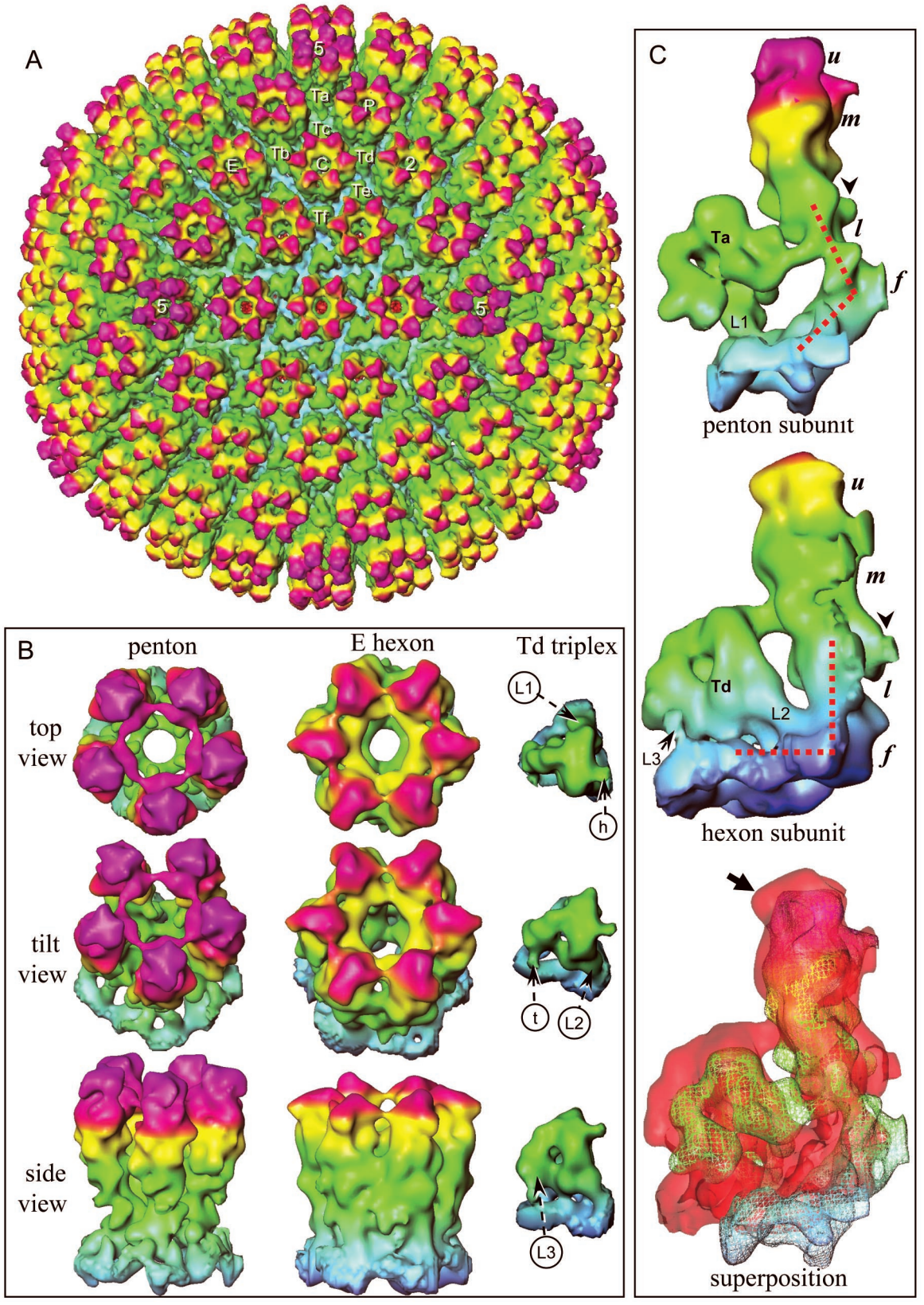

FIG. 5. RRV A capsid structure and subunit interactions at 15-Å resolution. See the legend to Fig. 3 for an explanation of color coding. (A) Shaded surface representation of the 3D map of the A capsid, reconstructed from 3,824 particles, as viewed along a twofold axis. Three pentons (5), three structurally unique hexons (P, E, and C), and six triplexes (Ta, Tb, Tc, Td, Te, and Tf, following the designations used for HSV-1) are labeled. (B) Top, tilt, and side views of a penton, an E hexon, and a Td triplex, computationally extracted from the A capsid reconstruction shown

duced capsids that disassembled at the nonpermissive temperature of 0°C, similar to the in vitro-assembled procapsids (40). The capsids matured when protease activity was restored (40), demonstrating that the procapsid is the precursor of the angular capsid. The proteolytic cleavage of the intracapsid scaffolding proteins at their C termini by the viral protease (19, 22, 23, 36) interrupts scaffolding protein-MCP interactions (63). This is followed by the recruiting of the smallest capsid protein VP26 through an ATP-dependent process (12), leading to the formation of the intermediate or B capsids. It has not been shown whether the B capsid, or the procapsid, or a yet-unknown intermediate capsid form, can package DNA, with the simultaneous exit of the cleaved scaffolding protein, forming the C capsid. The A capsid is empty and represents a nonfunctional by-product of either the loss of a scaffolding protein from a B capsid without concomitant DNA packaging, or the loss of viral genomic DNA from a C capsid (31). The C capsid buds through the nuclear membrane through an envelopment and deenvelopment process and acquires an additional layer of proteins that forms the tegument in the cytoplasm (see reference 25 for a review). Enveloped virions are then released by exocytosis.

Whether gammaherpesviruses use a similar viral assembly mechanism and maturation pathway remained hitherto unaddressed, owing to difficulties in isolating adequate amounts of the different types of KSHV and EBV capsids for biochemical and structural characterization. The cryoEM images of the RRV A, B, and C capsids (Fig. 2) closely resemble those of HSV-1 (5, 44, 59, 64) and human CMV (8), members of the alpha- and betaherpesvirus subfamilies, respectively. As expected, the RRV capsids are also similar to those of KSHV in negative-stain electron microscopy (27) and cryoEM (51, 56) and in chemical compositions (35a). The similarity of RRV and alphaherpesvirus capsids in both structural organization and chemical compositions (35a) suggests that gammaherpesvirus capsid assembly and maturation probably proceed in a manner similar to that in alphaherpesviruses.

The hallmarks of the RRV B capsid reconstruction resemble those observed in the HSV-1 B capsid in many aspects. First, the RRV scaffolding core exhibits no significant icosahedral symmetry, as judged from the poor resolution of the core densities, but its radial density distribution suggests that it can be divided into three sublayers, similar to those of the scaffolding core in HSV-1 (50). Such a structure may have an extended and flexible conformation, which would account for the unresolved structure in our reconstructions of this region inside the capsid. This notion is consistent with the proposal that both the middle and N-terminal domains of SCAF promote self-aggregation within the B capsids to form the middle and inner scaffold layers, respectively, as suggested for the HSV-1 scaffolding protein (28, 31). The outer layer of the scaffold appears to have some disordered densities that directly extend from or are linked to the middle layer by a more flexible linker. The high flexibility and mobility of the outer layer may play a critical role in allowing the symmetrically arranged MCP to interact with the nonsymmetric scaffold to define the size and shape of the capsid during the early stages of capsid assembly.

In addition to presenting direct structural evidence demonstrating a similar capsid assembly pathway shared by gammaherpesvirus and alphaherpesvirus capsids, our study represents the first time that the 3D structures of all three types of herpesvirus capsids were systematically compared at identical resolutions. This work has allowed the distinction of subtle structural differences, such as penton channel configurations, which were not addressed previously. Moreover, the structure of the RRV A capsid at a 15-Å resolution is the highest-resolution structure achieved for a gammaherpesvirus capsid to date, and the data have allowed the identification of structural features unique to gammaherpesvirus capsids (see below) that could not be seen in the previously published 24-Å structures of KSHV capsids (51, 56).

Structural comparisons of capsid proteins of alpha-, beta-, and gammaherpesviruses. The 15-Å resolution of the RRV A capsid structure in the present study revealed that penton and hexon subunits have a nearly identical elongated shape that is dimensionally similar to those of HSV-1 and human CMV. The correlation of the biochemical and structural results suggests that the pentons and hexons of the RRV capsids are composed of five and six copies of MCP, respectively. In HSV-1 and KSHV, the smallest capsid protein has been shown to selectively bind to the hexon tips only (24, 52, 62, 64). Our reconstruction of the RRV A capsid suggests that RRV SCIP also binds to the hexon subunit but its presence or absence on pentons is less clear as illustrated in the comparison with HSV-1 and RRV penton subunit in Fig. 6 and its contour is much less prominent than its counterparts in HSV-1 and is almost unidentifiable at lower resolutions (cf. Fig. 5C and Fig. 5D and F in reference 56). This difference reinforces the observation that the most distinguishing structural characteristics of gammaherpesvirus capsids, compared with alpha- and betaherpesvirus capsids, lie at the distal ends of the pentons and hexons, the putative binding site(s) for SCIP, and the triplexes surrounding the pentons (i.e., Ta). This observation suggests possible differences in the association of the capsids with overlying tegument proteins and is reminiscent of such differences

in panel A. The subunits of both the penton and the hexon have similar elongated shapes. The three legs of the Td triplex are indicated by L1, L2, and L3. The three legs of the triplex are anchored to the capsid floor and interact with adjacent hexons and pentons with head (h) and tail (t) protrusions, respectively. (C) Side views of regions containing one penton subunit or one hexon subunit and its associated triplex (Ta or Td, respectively), computationally extracted from the A capsid reconstruction shown in panel A. The upper (u), middle (m), lower (l), and floor (f) domains of the penton or hexon subunits are labeled. The arrowheads indicate a density protrusion that forms a constriction inside the hexon channel and a corresponding density protrusion that does not form a constriction inside the penton channel. Triplex legs (L1, L2, and L3) connected to the floor domain of MCP are indicated; only L1 is connected in Ta. The red dotted lines on the lower and floor domains illustrate the angles between the two domains. The superposition of the penton (contour lines) and hexon (red semitransparent) subunits reveals an extra density (arrow) attached to the upper domain of each hexon subunit; this density could be attributed to SCIP. This putative SCIP density is structurally distinct from its homolog in HSV-1, the horn-shaped VP26 (52, 62, 64) (cf. this figure with Fig. 5D and F in reference 56). "2" and "5" indicate icosahedral 2- and 5-fold axes.

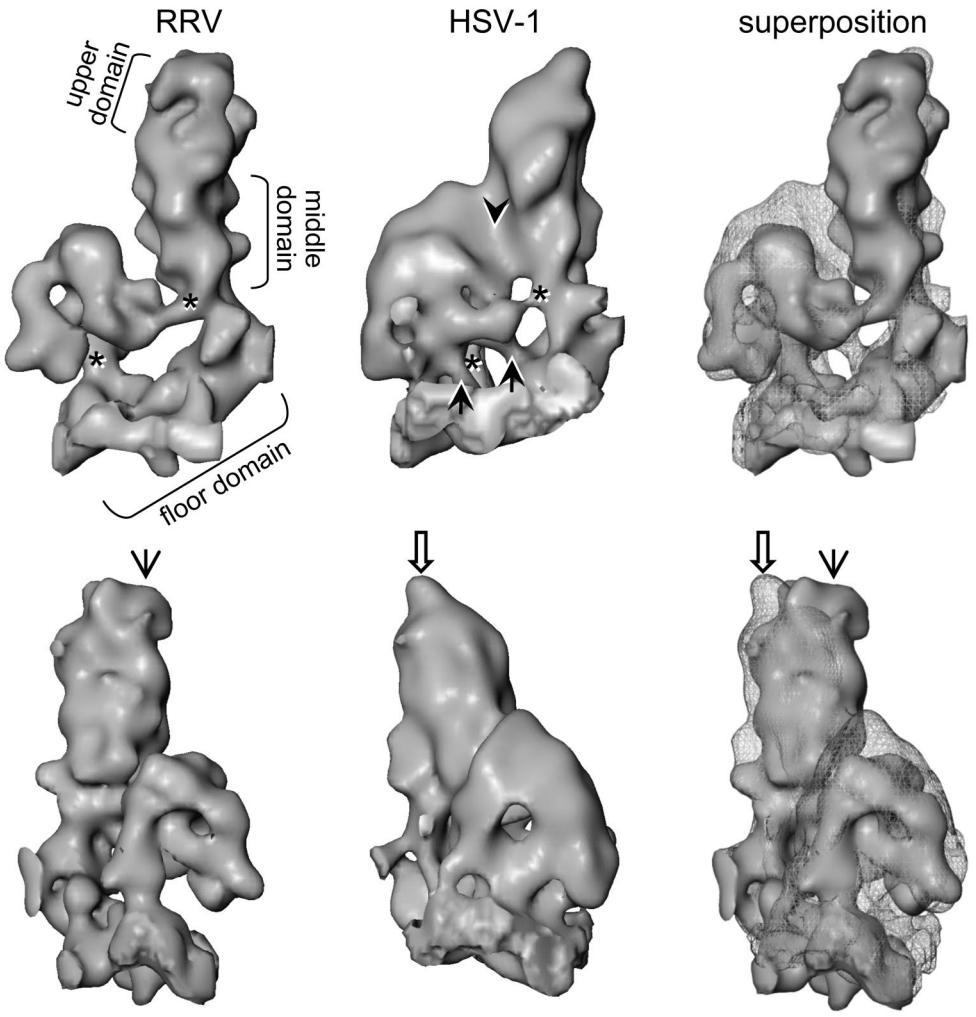

FIG. 6. Structural differences between RRV and HSV-1 capsids. A region encompassing one penton subunit and one triplex (Ta) was computationally extracted from the RRV A capsid reconstruction at 15-Å resolution and from an HSV-1 capsid reconstruction filtered to the same resolution from an 8.5-Å map (60). The maps were rotated for display such that the fivefold axis is approximately parallel to the longer edge of the page, and the views in the top and bottom rows are related to each other by an ~130° rotation about this axis. In the superposition views (right), the HSV-1 map is shown as wire frames. In both RRV and HSV-1, the Ta triplex interacts with MCP through the L1 leg connected to the MCP floor domain and through a small link to the MCP middle domain; these connections are indicated by asterisks. The major differences between the RRV and HSV-1 structures are indicated, including the interactions of triplex Ta with the middle domain of the penton subunit (arrowhead) and with the floor of the capsid (arrows) in HSV-1 and the absence of these interactions in RRV. The upper domain of the RRV capsid is square shaped and has an extra density (thin arrow in bottom row), while that of the HSV-1 penton subunit is diamond shaped (open arrow in bottom row). The HSV-1 penton subunit appears tilted slightly more toward the fivefold axis.

between human CMV and HSV-1 (11, 57). The reconstruction of the intact human CMV particles revealed a layer of highly organized filamentous densities of tegument proteins attached to the pentons, hexons, and triplexes of the underlying nucleocapsid (11). This extensive tegument-capsid association exhibited major differences from that of HSV-1, whose tegument proteins bind only to pentons and the surrounding triplexes (57). These structural disparities suggest that SCIP (or its homologs in other herpesvirus subfamilies) and some triplexes, together with tegument and glycoproteins, confer structural and functional specificities in alpha-, beta-, and gammaherpesviruses. Indeed, it has been shown that the human CMV UL48.5-encoded SCIP is essential for human CMV infection in vivo (6), but its HSV-1 counterpart, VP26, is dispensable for HSV-1 infection (10, 14).

In HSV-1, triplexes are heterotrimers composed of one copy of VP19C and two copies of VP23 (32, 34, 46, 64). SDS-PAGE revealed that the RRV capsids have two homologous proteins, TRI-1 and TRI-2, whose stain intensities on SDS-PAGE gels are consistent with a 1:2 molar ratio (Fig. 1) (35a). The 15-Å RRV A capsid reconstruction reveals that two of the three legs in each triplex are similar, except for Tf (Fig. 5A and C), which is located on the threefold axis; this organization is analogous to that of alpha- and betaherpesviruses, indicating that the overall structure of the triplexes is preserved across different herpesviruses. Thus, as with HSV-1, each RRV triplex is likely also composed of heterotrimers with one copy of TRI-1 and two copies of TRI-2, the homologs of VP19C and VP23, respectively. Except for the symmetric Tf and structurally unique Ta (see below), two (L1 and L2 in Fig. 5B) of the three legs are

similar in each RRV triplex and can be attributed to be a TRI-2 dimer. The third leg (L3 in Fig. 5B) probably corresponds to a TRI-1 monomer. Similar heterotriplexes are present in KSHV (27, 56). In RRV, however, the six triplexes located at geometrically unique positions (and thus different environments) within an asymmetric unit of the capsid exhibit substantially more differences in their structures than those in HSV-1 capsids reported at similar resolution (59). In particular, RRV triplex Ta exhibits much less extensive interactions with its adjacent penton MCP than HSV-1 triplex Ta (Fig. 6).

Functional implications of the channels. The functional implications of the different states of the penton channels in the different capsid types are intriguing. During the process of gammaherpesvirus lytic replication, viral materials, such as viral DNA and the proteolytically cleaved scaffolding proteins, have to be transferred into and out of the preformed capsids, respectively, through existing channels or pores in the capsids. Our structure revealed that the RRV capsids have three types of channels or pores: the small hole underneath the triplex, the penton channel and the hexon channel. It is plausible that SCAF molecules exit through some of these channels after their cleavage. Our structures clearly show that the penton channel is closed in RRV B capsids but open in A and C capsids (Fig. 3C and D). Because of the lack of systematic comparisons of the structures of the A, B, and C capsids in alpha- and betaherpesviruses, as conducted in this study, a clear distinction between their channels has not been provided. The only published HSV-1 C capsid reconstruction did not resolve the penton channel, probably due to the relatively low resolution of the 3D reconstruction (5). However, the DNA-containing nucleocapsid in the intact HSV-1 virion has a closed penton channel (57).

Recent studies with HSV-1 have demonstrated that, as with many bacteriophages, the linear viral genome is likely to enter at a unique vertex known as the portal complex (33). Because our reconstructions of the RRV capsid structures do not take into account such asymmetry and, instead, treat all 12 vertices equally, we cannot rule out the possibility that the portal complex in the B capsid has an open channel for DNA entry, while the other 11 penton channels adopt a closed conformation, or that the closed penton channel may simply be an artifact arising from the averaging of 11 slightly open penton channels with a closed portal. Nevertheless, the functional significance of the closed penton channels in the B capsid reconstruction is probably related to retention of the scaffolding proteins rather than to the specific penton or portal complex used for packaging genome DNA. It is conceivable that if penton channels were indeed the release path of the cleaved scaffolding protein, they would be open to allow the completion of this process leading to the transformation from B to C capsid (after successful DNA encapsidation) or A capsid (after loss of DNA or a scaffolding protein). It is attractive to speculate that the encapsidation of DNA genome is coupled with the release of the scaffolding proteins. Thus, the functional role of a closed penton channel in the B capsid might be to prevent the premature release of the scaffolding proteins. Whether the penton channels in the nucleocapsid within the RRV virion remain open is yet to be seen. The nucleocapsid within the HSV-1 virion, however, has closed penton channels (57). Therefore, the open penton channels in the RRV C capsid indicate that any closure of the penton channels does not take place immediately after the completion of scaffolding proteins release and DNA encapsidation. After the completion of DNA packaging, closure of the open penton channels would protect the inner DNA from premature release. The mechanism for regulating the penton channel opening and closure is not known and is probably related to the differences in surface-charge properties, as reported recently for HSV-1 penton and hexon channels (7). In virions, it is also possible that this process of channel closing may involve one or more tegument proteins and may take place during the tegumentation period, when the C capsid further matures into the infectious virion. In addition, our 21-Å resolution C capsid reconstruction revealed that the outer layers of the packaged DNA have strongest connections with the inner face of the capsid floor around pentons.

Packaging of viral DNA in different herpesviruses. Previous studies of HSV-1 have shown that the genomic DNA within the nucleocapsid inside a virion is closely packaged into multiple shells of regularly spaced densities, with 26 Å between adjacent DNA duplexes (57). The central slice and radial density plot in Fig. 4 indicate that the RRV C capsid has an almost identical pattern of DNA organization, although slightly more compact, with a 25-Å interduplex distance. Although RRV capsids, like KSHV capsids, have nearly the same diameter as HSV-1 capsids (1250 Å), RRV has a slightly larger genome size than HSV-1, ~165 and 153 kb, respectively (1, 20, 37, 45). Therefore, the smaller interduplex distance may merely reflect the need to compact this greater amount of DNA into the same volume within the capsid. Buttressing this interpretation, human CMV has the largest genome (225 kb) of all human herpesviruses but has a capsid that is only slightly larger (1,300-Å diameter), and its DNA was shown to be packaged with an interduplex distance of only 23 Å (4). Based on the interduplex spacing and the genome sizes, we estimated that the closely packaged DNA genomes of HSV-1, RRV, and human CMV would occupy total volumes of 3.52×10^8, 3.51×10^8, and 4.05×10^8 Å^3, respectively (volume equals interstrand distance squared times the length of DNA, where the length of DNA is the number of base pairs times [3.4 Å/base pair]). These volumes would, in turn, occupy approximately 92, 92, and 90% of the total available spaces inside the HSV-1, RRV, and human CMV capsids, as estimated on the basis of their inner diameters of 900, 900, and 950 Å, respectively. The 23- to 26-Å packaging of strands of herpesviruses dsDNA is very close to the 20-Å diameter of B-type dsDNA, suggesting that herpesvirus genomes are packaged as "naked" DNA without any bound histone-like basic proteins. In this regard, SDS-PAGE analyses demonstrated that the A capsids and C capsids of either HSV-1 or RRV have the same protein compositions (5, 35a). In the absence of histone-like proteins, close packaging of naked DNA would lead to a potentially strong electrostatic repulsion between the juxtaposed negatively charged DNA duplexes. This, in turn, would make the packaging of DNA into B capsid energetically unfavorable, supporting the need for an energy-dependent DNA packaging machinery, such as the bacteriophage-like connector recently reported in HSV-1 capsids (33). Even so, it is conceivable that the negative charges of DNA may at least be partially neutralized by binding spermidine or some other heretofore undiscovered small basic molecules to reduce the strong electrostatic repulsion.

ACKNOWLEDGMENTS

Z.H.Z. and D.H.K. are Pew Scholars in Biomedical Sciences (Pew Charitable Trusts). This research was supported in part by NIH grants CA94809 (to Z.H.Z.), AI46420 (to Z.H.Z.), CA88768-01 (to D.H.K.), CA096500 (to B.D.), and NIGMS T32GM008136 (to C.M.O.); Welch Foundation grant AU-1492 (to Z.H.Z.); American Heart Association grant 0240216N (to Z.H.Z.); and Doris Duke Charitable Foundation Award 20000355 (to D.H.K.).

We thank Wah Chiu and Frazer Rixon for the use of HSV-1 data and Pierrette Lo for careful reading of the manuscript.

REFERENCES

1. **Alexander, L., L. Denekamp, A. Knapp, M. R. Auerbach, B. Damania, and R. C. Desrosiers.** 2000. The primary sequence of rhesus monkey rhadinovirus isolate 26–95: sequence similarities to Kaposi's sarcoma-associated herpesvirus and rhesus monkey rhadinovirus isolate 17577. J. Virol. **74:**3388–3398.
2. **Baker, T. S., W. W. Newcomb, F. P. Booy, J. C. Brown, and A. C. Steven.** 1990. Three-dimensional structures of maturable and abortive capsids of equine herpesvirus 1 from cryoelectron microscopy. J. Virol. **64:**563–573.
3. **Berman, H. M., J. Westbrook, Z. Feng, G. Gilliland, T. N. Bhat, H. Weissig, I. N. Shindyalov, and P. E. Bourne.** 2000. The Protein Data Bank. Nucleic Acids Res. **28:**235–242.
4. **Bhella, D., F. J. Rixon, and D. J. Dargan.** 2000. Cryomicroscopy of human cytomegalovirus virions reveals more densely packed genomic DNA than in herpes simplex virus type 1. J. Mol. Biol. **295:**155–161.
5. **Booy, F. P., W. W. Newcomb, B. L. Trus, J. C. Brown, T. S. Baker, and A. C. Steven.** 1991. Liquid-crystalline, phage-like packing of encapsidated DNA in herpes simplex virus. Cell **64:**1007–1015.
6. **Borst, E. M., S. Mathys, M. Wagner, W. Muranyi, and M. Messerle.** 2001. Genetic evidence of an essential role for cytomegalovirus small capsid protein in viral growth. J. Virol. **75:**1450–1458.
7. **Bowman, B. R., M. L. Baker, F. J. Rixon, W. Chiu, and F. A. Quiocho.** 2003. Structure of the herpesvirus major capsid protein. EMBO J. **22:**757–765.
8. **Butcher, S. J., J. Aitken, J. Mitchell, B. Gowen, and D. J. Dargan.** 1998. Structure of the human cytomegalovirus B capsid by electron cryomicroscopy and image reconstruction. J. Struct. Biol. **124:**70–76.
9. **Carbone, A.** 2003. Emerging pathways in the development of AIDS-related lymphomas. Lancet Oncol. **4:**22–29.
10. **Chen, D. H., J. Jakana, D. McNab, J. Mitchell, Z. H. Zhou, M. Dougherty, W. Chiu, and F. J. Rixon.** 2001. The pattern of tegument-capsid interaction in the herpes simplex virus type 1 virion is not influenced by the small hexon-associated protein VP26. J. Virol. **75:**11863–11867.
11. **Chen, D. H., H. Jiang, M. Lee, F. Liu, and Z. H. Zhou.** 1999. Three-dimensional visualization of tegument/capsid interactions in the intact human cytomegalovirus. Virology **260:**10–16.
12. **Chi, J. H., and D. W. Wilson.** 2000. ATP-dependent localization of the herpes simplex virus capsid protein VP26 to sites of procapsid maturation. J. Virol. **74:**1468–1476.
13. **Crowther, R. A.** 1971. Procedures for three-dimensional reconstruction of spherical viruses by Fourier synthesis from electron micrographs. Philos. Trans. R. Soc. Lond. B **261:**221–230.
14. **Desai, P., N. A. DeLuca, and S. Person.** 1998. Herpes simplex virus type 1 VP26 is not essential for replication in cell culture but influences production of infectious virus in the nervous system of infected mice. Virology **247:**115–124.
15. **Desrosiers, R. C., V. G. Sasseville, S. C. Czajak, X. Zhang, K. G. Mansfield, A. Kaur, R. P. Johnson, A. A. Lackner, and J. U. Jung.** 1997. A herpesvirus of rhesus monkeys related to the human Kaposi's sarcoma-associated herpesvirus. J. Virol. **71:**9764–9769.
16. **DeWire, S. M., M. A. McVoy, and B. Damania.** 2002. Kinetics of expression of rhesus monkey rhadinovirus (RRV) and identification and characterization of a polycistronic transcript encoding the RRV Orf50/Rta, RRV R8, and R8.1 genes. J. Virol. **76:**9819–9831.
17. **Dougherty, M., and W. Chiu.** 2000. Macromolecular structure visualization tools at NCMI. Microsc. Microanal. **6:**282–283.
18. **Earnshaw, W. C., and S. C. Harrison.** 1977. DNA arrangement in isometric phage heads. Nature **268:**598–602.
19. **Hong, Z., M. Beaudet-Miller, J. Durkin, R. Zhang, and A. D. Kwong.** 1996. Identification of a minimal hydrophobic domain in the herpes simplex virus type 1 scaffolding protein which is required for interaction with the major capsid protein. J. Virol. **70:**533–540.
20. **Lagunoff, M., and D. Ganem.** 1997. The structure and coding organization of the genomic termini of Kaposi's sarcoma-associated herpesvirus. Virology **236:**147–154.
21. **Liang, Y., E. Y. Ke, and Z. H. Zhou.** 2002. IMIRS: a high-resolution 3D reconstruction package integrated with a relational image database. J. Struct. Biol. **137:**292–304.
22. **Liu, F., and B. Roizman.** 1992. Differentiation of multiple domains in the herpes simplex virus 1 protease encoded by the UL26 gene. Proc. Natl. Acad. Sci. USA **89:**2076–2080.
23. **Liu, F. Y., and B. Roizman.** 1991. The herpes simplex virus 1 gene encoding a protease also contains within its coding domain the gene encoding the more abundant substrate. J. Virol. **65:**5149–5156.
24. **Lo, P., X. Yu, I. Atanasov, B. Chandran, and Z. H. Zhou.** 2003. Three-dimensional localization of pORF65 in Kaposi's sarcoma-associated herpesvirus capsid. J. Virol. **77:**4291–4297.
25. **Mettenleiter, T. C.** 2002. Herpesvirus assembly and egress. J. Virol. **76:**1537–1547.
26. **Mueller, N.** 1999. Overview of the epidemiology of malignancy in immune deficiency. J. Acquir. Immune Defic. Syndr. **21:**S5–S10.
27. **Nealon, K., W. W. Newcomb, T. R. Pray, C. S. Craik, J. C. Brown, and D. H. Kedes.** 2001. Lytic replication of Kaposi's sarcoma-associated herpesvirus results in the formation of multiple capsid species: isolation and molecular characterization of A, B, and C capsids from a gammaherpesvirus. J. Virol. **75:**2866–2878.
28. **Newcomb, W. W., and J. C. Brown.** 1991. Structure of the herpes simplex virus capsid: effects of extraction with guanidine hydrochloride and partial reconstitution of extracted capsids. J. Virol. **65:**613–620.
29. **Newcomb, W. W., and J. C. Brown.** 1989. Use of Ar^+ plasma etching to localize structural proteins in the capsid of herpes simplex virus type 1. J. Virol. **63:**4697–4702.
30. **Newcomb, W. W., J. C. Brown, F. P. Booy, and A. C. Steven.** 1989. Nucleocapsid mass and capsomer protein stoichiometry in equine herpesvirus 1: scanning transmission electron microscopic study. J. Virol. **63:**3777–3783.
31. **Newcomb, W. W., F. L. Homa, D. R. Thomsen, F. P. Booy, B. L. Trus, A. C. Steven, J. V. Spencer, and J. C. Brown.** 1996. Assembly of the herpes simplex virus capsid: characterization of intermediates observed during cell-free capsid formation. J. Mol. Biol. **263:**432–446.
32. **Newcomb, W. W., F. L. Homa, D. R. Thomsen, B. L. Trus, N. Cheng, A. Steven, F. Booy, and J. C. Brown.** 1999. Assembly of the herpes simplex virus procapsid from purified components and identification of small complexes containing the major capsid and scaffolding proteins. J. Virol. **73:**4239–4250.
33. **Newcomb, W. W., R. M. Juhas, D. R. Thomsen, F. L. Homa, A. D. Burch, S. K. Weller, and J. C. Brown.** 2001. The UL6 gene product forms the portal for entry of DNA into the herpes simplex virus capsid. J. Virol. **75:**10923–10932.
34. **Newcomb, W. W., B. L. Trus, F. P. Booy, A. C. Steven, J. S. Wall, and J. C. Brown.** 1993. Structure of the herpes simplex virus capsid: molecular composition of the pentons and the triplexes. J. Mol. Biol. **232:**499–511.
35. **Newcomb, W. W., B. L. Trus, N. Cheng, A. C. Steven, A. K. Sheaffer, D. J. Tenney, S. K. Weller, and J. C. Brown.** 2000. Isolation of herpes simplex virus procapsids from cells infected with a protease-deficient mutant virus. J. Virol. **74:**1663–1673.

35a. **O'Connor, C. M., B. Damania, and D. H. Kedes.** 2003. De novo infection with rhesus monkey rhadinovirus leads to the accumulation of multiple intranuclear capsid species during lytic replication but favors the release of genome-containing virions. J. Virol. **77:**13439–13447.

36. **Preston, V. G., F. J. Rixon, I. M. McDougall, M. McGregor, and M. F. Al-Kobaisi.** 1992. Processing of the herpes simplex virus assembly protein ICP35 near its carboxy terminal end requires the product of the whole of the UL26 reading frame. Virology **186:**87–98.
37. **Renne, R., M. Lagunoff, W. Zhong, and D. Ganem.** 1996. The size and conformation of Kaposi's sarcoma-associated herpesvirus (human herpesvirus 8) DNA in infected cells and virions. J. Virol. **70:**8151–8154.
38. **Rixon, F. J.** 1993. Structure and assembly of herpesviruses. Semin. Virol. **4:**135–144.
39. **Rixon, F. J., M. D. Davison, and A. J. Davison.** 1990. Identification of the genes encoding two capsid proteins of herpes simplex virus type 1 by direct amino acid sequencing. J. Gen. Virol. **71:**1211–1214.
40. **Rixon, F. J., and D. McNab.** 1999. Packaging-competent capsids of a herpes simplex virus temperature-sensitive mutant have properties similar to those of in vitro-assembled procapsids. J. Virol. **73:**5714–5721.
41. **Roizman, B., and P. E. Pellett.** 2001. *Herpesviridae*: a brief introduction, p. 2381–2398. *In* B. N. Fields, D. M. Knipe, P. M. Howley, D. E. Griffin, R. A. Lamb, M. A. Martin, B. Roizman, and S. E. Strauss (ed.), Fields virology, 4th ed., vol. 2. Lippincott Williams & Wilkins, Philadelphia, Pa.
42. **Saad, A., Z. H. Zhou, J. Jakana, W. Chiu, and F. J. Rixon.** 1999. Roles of triplex and scaffolding proteins in herpes simplex virus type 1 capsid formation suggested by structures of recombinant particles. J. Virol. **73:**6821–6830.
43. **Schrag, J., B. Prasad, F. Rixon, and W. Chiu.** 1989. Three-dimensional structure of the HSV1 nucleocapsid. Cell **56:**561.
44. **Schrag, J. D., M. F. Schmid, D. G. Morgan, G. N. Phillips, Jr., W. Chiu, and L. Tang.** 1988. Crystallization and preliminary X-ray diffraction analysis of 11 S acetylcholinesterase. J. Biol. Chem. **263:**9795–9800.
45. **Searles, R. P., E. P. Bergquam, M. K. Axthelm, and S. W. Wong.** 1999. Sequence and genomic analysis of a rhesus macaque rhadinovirus with similarity to Kaposi's sarcoma-associated herpesvirus/human herpesvirus 8. J. Virol. **73:**3040–3053.
46. **Spencer, J. V., W. W. Newcomb, D. R. Thomsen, F. L. Homa, and J. C. Brown.** 1998. Assembly of the herpes simplex virus capsid: preformed triplexes bind to the nascent capsid. J. Virol. **72:**3944–3951.
47. **Steven, A. C., and P. G. Spear.** 1997. Herpesvirus capsid assembly and

envelopment, p. 312–351. *In* W. Chiu, R. M. Burnett, and R. Garcea (ed.), Structural biology of viruses. Oxford University Press, New York, N.Y.
48. **Tatman, J. D., V. G. Preston, P. Nicholson, R. M. Elliott, and F. J. Rixon.** 1994. Assembly of herpes simplex virus type 1 capsids using a panel of recombinant baculoviruses. J. Gen. Virol. **75:**1101–1113.
49. **Thomsen, D. R., L. L. Roof, and F. L. Homa.** 1994. Assembly of herpes simplex virus (HSV) intermediate capsids in insect cells infected with recombinant baculoviruses expressing HSV capsid proteins. J. Virol. **68:**2442–2457.
50. **Trus, B. L., F. P. Booy, W. W. Newcomb, J. C. Brown, F. L. Homa, D. R. Thomsen, and A. C. Steven.** 1996. The herpes simplex virus procapsid: structure, conformational changes upon maturation, and roles of the triplex proteins VP19c and VP23 in assembly. J. Mol. Biol. **263:**447–462.
51. **Trus, B. L., J. B. Heymann, K. Nealon, N. Cheng, W. W. Newcomb, J. C. Brown, D. H. Kedes, and A. C. Steven.** 2001. Capsid structure of Kaposi's sarcoma-associated herpesvirus, a gammaherpesvirus, compared to those of an alphaherpesvirus, herpes simplex virus type 1, and a betaherpesvirus, cytomegalovirus. J. Virol. **75:**2879–2890.
52. **Trus, B. L., F. L. Homa, F. P. Booy, W. W. Newcomb, D. R. Thomsen, N. Cheng, J. C. Brown, and A. C. Steven.** 1995. Herpes simplex virus capsids assembled in insect cells infected with recombinant baculoviruses: structural authenticity and localization of VP26. J. Virol. **69:**7362–7366.
53. **Trus, B. L., W. W. Newcomb, F. P. Booy, J. C. Brown, and A. C. Steven.** 1992. Distinct monoclonal antibodies separately label the hexons or the pentons of herpes simples virus capsid. Proc. Natl. Acad. Sci. USA **89:**11508–11512.
54. **Walters, J. N., G. L. Sexton, J. M. McCaffery, and P. Desai.** 2003. Mutation of single hydrophobic residue I27, L35, F39, L58, L65, L67, or L71 in the N terminus of VP5 abolishes interaction with the scaffold protein and prevents closure of herpes simplex virus type 1 capsid shells. J. Virol. **77:**4043–4059.
55. **Warner, S. C., G. Chytrova, P. Desai, and S. Person.** 2001. Mutations in the N-terminus of VP5 alter its interaction with the scaffold proteins of herpes simplex virus type 1. Virology **284:**308–316.
56. **Wu, L., P. Lo, X. Yu, J. K. Stoops, B. Forghani, and Z. H. Zhou.** 2000. Three-dimensional structure of the human herpesvirus 8 capsid. J. Virol. **74:**9646–9654.
57. **Zhou, Z. H., D. H. Chen, J. Jakana, F. J. Rixon, and W. Chiu.** 1999. Visualization of tegument-capsid interactions and DNA in intact herpes simplex virus type 1 virions. J. Virol. **73:**3210–3218.
58. **Zhou, Z. H., and W. Chiu.** 2003. Determination of icosahedral virus structures by electron cryomicroscopy at subnanometer resolution. Adv. Protein Chem. **64:**93–124.
59. **Zhou, Z. H., W. Chiu, K. Haskell, H. Spears, Jr., J. Jakana, F. J. Rixon, and L. R. Scott.** 1998. Refinement of herpesvirus B-capsid structure on parallel supercomputers. Biophys. J. **74:**576–588.
60. **Zhou, Z. H., M. Dougherty, J. Jakana, J. He, F. J. Rixon, and W. Chiu.** 2000. Seeing the herpesvirus capsid at 8.5 Å. Science **288:**877–880.
61. **Zhou, Z. H., S. Hardt, B. Wang, M. B. Sherman, J. Jakana, and W. Chiu.** 1996. CTF determination of images of ice-embedded single particles using a graphics interface. J. Struct. Biol. **116:**216–222.
62. **Zhou, Z. H., J. He, J. Jakana, J. D. Tatman, F. J. Rixon, and W. Chiu.** 1995. Assembly of VP26 in herpes simplex virus-1 inferred from structures of wild-type and recombinant capsids. Nat. Struct. Biol. **2:**1026–1030.
63. **Zhou, Z. H., S. J. Macnab, J. Jakana, L. R. Scott, W. Chiu, and F. J. Rixon.** 1998. Identification of the sites of interaction between the scaffold and outer shell in herpes simplex virus-1 capsids by difference electron imaging. Proc. Natl. Acad. Sci. USA **95:**2778–2783.
64. **Zhou, Z. H., B. V. Prasad, J. Jakana, F. J. Rixon, and W. Chiu.** 1994. Protein subunit structures in the herpes simplex virus A-capsid determined from 400 kV spot-scan electron cryomicroscopy. J. Mol. Biol. **242:**456–469.